Journal of Nanobiotechnology

RESEARCH Open Access

Influences of lead-based perovskite nanoparticles exposure on early development of human retina

Cao Yang[1,2†], Zhulin Du[3†], Linqiang Mei[4,5], Xia Chen[1,2], You Liao[4,5], Lingling Ge[1,2], Jiahui Kang[1,2], Zhanjun Gu[4,5*], Xiaotang Fan[3*] and Haiwei Xu[1,2*]

Abstract

Background Lead-based perovskite nanoparticles (Pb-PNPs) are widely utilized in the photovoltaic industry. However, due to their poor stability and high water solubility, lead often gets released into the environment, which can negatively impact the development of the central nervous system (CNS). As an extension of the CNS, the effects and mechanisms of Pb-PNPs on human retinal development have remained elusive.

Objectives We aimed to investigate the effects of Pb-PNPs on human retinal development.

Methods Human embryonic stem cell-derived three-dimensional floating retinal organoids (hEROs) were established to simulate early retinal development. Using immunofluorescence staining, biological-transmission electron microscopy analysis, inductively coupled plasma-mass spectrometry, two-dimensional element distribution detection, and RNA sequencing, we evaluated and compared the toxicity of $CsPbBr_3$ nanoparticles (a representative substance of Pb-PNPs) and $Pb(AC)_2$ and investigated the toxicity-reducing effects of SiO_2 encapsulation.

Results Our findings revealed that $CsPbBr_3$ nanoparticles exposure resulted in a concentration-dependent decrease in the area and thickness of the neural retina in hEROs. Additionally, $CsPbBr_3$ nanoparticles exposure hindered cell proliferation and promoted cell apoptosis while suppressing the retinal ganglion cell differentiation, an alteration that further led to the disruption of retinal structure. By contrast, $CsPbBr_3$ nanoparticles exposure to hEROs was slightly less toxic than $Pb(AC)_2$. Mechanistically, $CsPbBr_3$ nanoparticles exposure activated endoplasmic reticulum stress, which promoted apoptosis by up-regulating Caspase-3 and inhibited retinal ganglion cell development by down-regulating Pax6. Interestingly, after coating $CsPbBr_3$ nanoparticles with silica, it exhibited lower toxicities to hEROs by alleviating endoplasmic reticulum stress.

†Cao Yang and Zhulin Du contributed equally to this work.

*Correspondence:
Zhanjun Gu
zjgu@ihep.ac.cn
Xiaotang Fan
fanxiaotang@tmmu.edu.cn
Haiwei Xu
xuhaiwei@tmmu.edu.cn

Full list of author information is available at the end of the article

Conclusion Overall, our study provides evidence of Pb-PNPs-induced developmental toxicity in the human retina, explores the potential mechanisms of $CsPbBr_3$ nanoparticles' developmental toxicity, and suggests a feasible strategy to reduce toxicity.

Graphical abstract

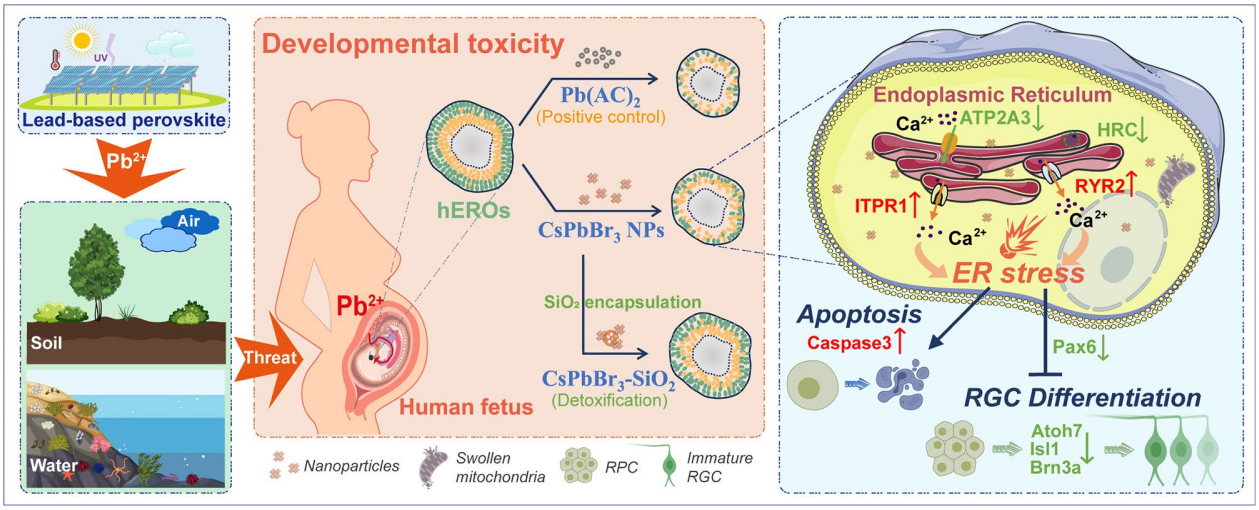

Keywords Lead-based perovskite nanoparticles, Retina, Developing, Toxicity, Organoids, Prenatal lead exposure

Background

Halide perovskite nanoparticles (PNPs) have shown great potential as photovoltaic materials.[1, 2] Of all the PNPs, lead-based perovskite nanoparticles (Pb-PNPs) are especially promising due to their high photovoltaic conversion efficiency [3]. Pb-PNPs have been extensively utilized in different applications, including perovskite solar cells [4], light-emitting diodes [5], photoelectric detector [6], X-ray microscopic imaging [7], and more.[8, 9] It is clear that Pb-PNPs will continue to be produced and utilized on a large scale.

Due to its poor stability and high water solubility, this material can release significant amounts of lead during its manufacturing, working, and recycling processes [3, 10, 11]. As lead is released into water and soil, it threatens the environment and human health [12–14]. It has shown that the toxicity of Pb-PNPs is primarily caused by lead ions (Pb^{2+}) [15, 16], a pervasive environmental toxicant known to interfere with the development of the CNS [17]. Meanwhile, previous research has demonstrated that Pb can cross the placental barrier and impact fetal brain development [18], resulting in long-lasting effects on retinal photoreceptors in children [19]. The retina, an extension of the CNS, is particularly vulnerable to toxic damage during its developmental process [19–22]. While the nanoscale size of Pb-PNPs may cause inconsistent biological effects compared to conventional Pb ions, the impact of Pb-PNPs exposure on early retinal development remains unclear. Most studies on Pb exposure have been conducted using zebrafish [16], rat [23], mouse [24], and cellular [24] models. Therefore, there is also an urgent need for an appropriate model to simulate early human embryonic retinal development.

Encouragingly, three-dimensional floating human retinal organoids can simulate early retinal development in vitro [25]. Organoids have similar efficacy as in vivo models for toxicity assessment [26]. A previous study evaluated the effect of environmental stimuli on early retinal development by applying hEROs [21]. Three-dimensional floating organoid models also show significant advantages in nanoparticle safety assessment [27]. Therefore, this model holds great promise in evaluating the effect of Pb-PNPs on early retinal development.

This study assessed the potential adverse effects of early exposure to $CsPbBr_3$ nanoparticles, a substance common to Pb-PNPs. To conduct this research, we used advanced techniques such as laser ablation-inductively coupled plasma-time-of-flight mass spectrometry (LA-ICP-TOFMS), inductively coupled plasma mass spectrometry (ICP-MS), RNA sequence, and biological analysis.

Materials and methods

Preparation and characterization analysis

Chemicals. Cesium bromide (CsBr, 99.999%), lead bromide ($PbBr_2$, 99.999%), tetraethoxysilane (TEOS, 98%), and N, N-dimethylformamide (DMF, 99.9%) were provided by Alfa Aesar. Oleic acid (OA, 90% tech), oleylamine (OAm), and toluene (99.95%) were obtained

from Sigma-Aldrich. A 4% paraformaldehyde solution was provided by Boster Biological Technology Co., Ltd. BV-III grade Nitric acid (HNO_3, 70%), and ethanol were obtained from Beijing Chemical Corporation. All chemicals were used directly.

Preparation of $CsPbBr_3$and $CsPbBr_3$-SiO_2nanoparticles. The 734 mg of $PbBr_2$, 425 mg of CsBr, 3 mL of OAm, and 9 mL of OA were added into 50 mL of DMF, stirring at 1200 rpm and heating at 110 °C. After 3 h, 1 mL ammonia solution (2.8%) was dropwise added to obtain a clear precursor solution. Moreover, 20 mL of the above solution was quickly added into toluene. And the solution turned green, indicating the formation of $CsPbBr_3$ nanoparticles. Additionally, 20 mL of the precursor solution was quickly added into toluene containing 200 µL of TEOS. $CsPbBr_3$-SiO_2 nanoparticles were obtained by stirring vigorously for 10 s and stirring at 150 rpm for 2 h. The $CsPbBr_3$ nanoparticles or $CsPbBr_3$-SiO_2 nanoparticles were washed three times with toluene, centrifugated at 12,000 rpm, and stored in a vacuum box for further experimentation.

Characterizations. Transmission electron microscope (TEM) images were obtained by a JEM-2100plus TEM. Powder X-ray diffraction (XRD) analysis was carried out by a Bruker D8 advance diffractometer with Cu Kα radiation (λ = 1.5418 Å). Energy-dispersive X-ray spectroscopy (EDS, Horiba 7593-H model) in conjunction with a field-emission scanning electron microscope (FE-SEM, S-4800, Hitachi High Technologies, Japan) was used to determine the composition and morphology of the samples. X-ray photoelectron spectroscopy (XPS) analysis was collected on an ESCALab220i-XL. Fourier transform infrared (FTIR) spectra were recorded with a Bruker Vertex 70 spectrometer.

hESCs culturing and generation of hEROs

The human embryonic stem cell (hESC) line (H9) used was kindly provided by the Stem Cell Bank, Chinese Academy of Sciences (CAS). hESCs were cultured in feeder-free Essential 8™ Culture Medium (A1517001, Gibco). The generation of the retina organoid followed Kuwahara's protocol [28] with slight modifications as described in our earlier study [29]. Briefly, confluent hESCs were dissociated into a single-cell suspension using TrypLE™ Express (12605028, Gibco). hESCs (1.2×10^4, 100µL) were forced to aggregate into embryoid body (EB) formation in low-adhesion V-shaped bottom 96-well plates (MS-9096VZ, Sumitomo Bakelite) in growth factor-free chemically defined medium (gfCDM) supplemented with 10% KnockOut™ Serum Replacement (KSR) (A3181502, Gibco), 20µM Y-27632 (the ROCK inhibitor) (Sigma), and 1% penicillin-streptomycin (SV30010, Hyclone). gfCDM contains 45% Iscove's modified Dulbecco's medium (IMDM) (12440053, Gibco), 45% Ham's F12-Glutamax (31765035, Gibco), 1% Chemically Defined Lipid Concentrate (Gibco), and monothioglycerol (450 µM) (Sigma). After five-day induction, the culture medium was exchanged for fresh gfCDM (without Y-27632) supplemented with 1.5 nM bone morphogenetic protein 4 (BMP4) (Peprotech, United States). After this, half of the gfCDM was changed every three days. On day 18, hEROs were transferred to an ultra-low attachment dish (752001, NEST) for further culture with long-term culture medium containing Dulbecco's modified Eagle's medium (DMEM)/F12 (10565018, Gibco), 1% N2 supplement (A1370701, Gibco), 10% fetal bovine serum (FBS), (35–081, Corning), 0.5 µM retinoic acid (RA) (R2625, Sigma), 0.1 mM taurine (T8691, Sigma), and 1% penicillin-streptomycin (SV30010, Hyclone).

Preparation of exposed solution and determination of actual concentration

Recent studies have shown that the blood lead levels of pregnant women range from 0.023 to 0.348 µg/ml, and umbilical cord blood levels range from 0.021 to 0.45 µg/ml [30]. Furthermore, stored lead in the mother's body during pregnancy can be released into the bloodstream and passed on to the fetus [31]. Given this, we have prepared the following solution. $Pb(AC)_2$ (CAS: 6080-56-4, L812500, MACKLIN, China), $CsPbBr_3$, and $CsPbBr_3$-SiO_2 nanoparticles were prepared at a stock concentration of 100 mg/ml in dimethyl sulfoxide (DMSO, D8371, Solarbio, China). A diluted concentration of 25 µg/ml, 50 µg/ml and 100 µg/ml was added to the medium. Then, we detected the working concentration of $Pb2^+$ in the culture medium using ICP-MS, and the specific data can be found in Supplementary Fig. 2. The ICP-MS data showed that the actual Pb^{2+} concentration of the preset low-concentration $CsPbBr_3$ nanoparticles group is approximately 0.12 µg/ml, which is at the physiological high value of maternal blood lead levels.

Materials exposure experiments

Following the hEROs were cultured in long-term culture medium (D18), they were assigned to four groups: (i) the control group, (ii) the low-concentration $CsPbBr_3$ nanoparticle group (actual lead content about 0.12 µg/ml) (CPBL), (iii) the middle-concentration $CsPbBr_3$ nanoparticle group (actual lead content about 0.30 µg/ml) (CPBM), (iv) the high- concentration $CsPbBr_3$ nanoparticle group (actual lead content about 0.57 µg/ml) (CPBH) for toxicity assays. In this study, hEROs were also exposed to different chemicals with the same low preset concentration, including $CsPbBr_3$-SiO_2 (actual lead content about 0.06 µg/ml), and $Pb(AC)_2$ (actual lead content about 0.23 µg/ml), respectively. Detailed measurement data can be found in the supplementary materials (Fig. S2). To ensure the accuracy of the concentrations used,

medium and corresponding concentration nanoparticles and chemicals were refreshed every three days.

hEROs morphological observations and analysis

The morphology and growth of the hEROs were observed and photographed weekly by a Leica DMI3000 B inverted microscope (Leica, Germany). Following the nanoparticle exposure periods, the morphological changes in the neural retina (NR) of hEROs were identified and quantified. We have referenced previously published articles for measuring the area and thickness of the NR [26, 32]. The specific method for measuring the area and thickness of the NR is as follows: in the hERO images obtained with the microscope, the area of the NR for each hERO was measured by using ImageJ(64-bit) software (NIH, Bethesda, MD, United States). Moreover, we measured the thickness of the NR at ten points (distributed as evenly as possible) in the hEROs of the control and experimental groups, ensuring that measurements were not taken at the ciliary edge of the NR. Then, the average of these ten measurements was calculated to obtain the thickness of the NR.

Immunofluorescence staining

Immunostaining of hEROs was consistent with the description in our previous study [32]. hEROs were collected and fixed with 4% paraformaldehyde (P0099, Beyotime) at 4 °C for 20 min, followed by dehydration in 30% sucrose (1245GR500, Biofroxx) at 4 °C. hEROs were then embedded in optimal cutting temperature (OCT) compound (Sakura FineTek, Torrance, CA, United States) and transferred into − 80 °C refrigerator. hEROs were cut on a freezing microtome (Leica CM1900UV, Germany) into 12 μm thick sections and mounted onto glass slides. Frozen sections were then stored at -20 °C in a refrigerator until immunostaining. Slides were incubated in PBS at 37 °C for 20 min to remove OCT. Slides were then permeabilized in 0.5% Triton X-100 for 15 min at room temperature. Nonspecific sites were blocked with 3% bovine serum albumin (BSA) in a moist chamber at 37 °C for 30 min. Slides were then sequentially incubated with primary antibodies (see Table S1) at 4 °C overnight. The following day, sections were incubated for 60 min at 37 °C with the appropriate Alexa Fluor dye-conjugated secondary antibodies, including Goat anti-mouse IgG Alexa-Fluor-488 (A11001, Life technologies, 1:400), Goat anti-mouse IgG Alexa-Fluor-568 (A11031, Life technologies, 1:500), Goat anti-rabbit IgG Alexa-Fluor-488 (A11008, Life technologies, 1:400), or Goat anti-rabbit IgG Alexa-Fluor-568 (A11011, Life technologies, 1:500), following washing the sections with 1 × PBS three times every 10 min. Finally, DAPI (C1006, Beyotime) dye was applied for nuclear counterstaining for 10 min at room temperature and coverslips were mounted with anti-fluorescence quenching sealer (P0126, Beyotime). Zeiss inspected and photographed the slides using an LSM880/LSM780 confocal microscope, and the images were analyzed using the Zen 2012 software version.

TUNEL assays

After three weeks of exposure to nanoparticles, samples from both the control and exposure groups were collected and prepared for frozen sections. Apoptosis of neural layer cells was assessed using a TUNEL kit (Roche, Switzerland). The end-labeling enzyme and labeling liquid were mixed at a ratio of 1:9 according to the instructions, after which the sections were incubated with the sections at 37 °C protected from light for one hour, followed by incubation with DAPI for 10 min. Photographs were taken using a laser confocal microscope (Zeiss, LSM880 and LSM780). The images were then analyzed using Zen 2012.

Biological-transmission electron microscopy (Bio-TEM) analysis

hEROs were exposed to $Pb(AC)_2$, $CsPbBr_3$, and $CsPbBr_3$-SiO_2 nanoparticles for three weeks. Meanwhile, the normal cultured hEROs served as the control group. On Day 39, the samples from each group were collected. Subsequently, they were washed three times with PBS and then fixed with 2.5% glutaraldehyde. They were further fixed using osmium acid, dehydrated, embedded, sectioned, and stained. The prepared samples were then examined using an electron microscope (Hitachi HT7800) to observe the biodistribution of nanomaterials and the intracellular structure of each group of cells.

Two-dimensional element distribution detection of organoids slices

The LA-ICP-TOFMS technique analyzed the two-dimensional elemental distribution in hERO slices. Following various treatments, the hEROs were embedded in the OCT on a freezing stage, and frozen sections (12 μm) were obtained using a freezing microtome. Next, frozen sections of the hEROs were used for LA-ICP-TOFMS detection. The LA-ICP-TOFMS system consists of a Laser Ablation System (Iridia Bio, Teledyne Photon Machines) and an Inductively Coupled Plasma Time-of-Flight Mass Spectrometry system (icpTOF2R, TOFWERK).

Inductively coupled plasma-mass spectrometry (ICP-MS)

Pb, Br, and Cs concentrations of the day 39 hEROs were determined by ICP-MS. Briefly, the samples were collected and subjected to microwave digestion (Touchwin 2.0) using pure nitric acid, followed by heating at 180 °C for 30 min to drive off the acid. The concentration of the relevant elements was measured on the inductively coupled plasma mass spectrometer (NexION300D, PE, U.S.) after filtering the impurities using a 0.22 μm filter membrane.

RNA sequencing

To comprehensively evaluate the toxic effects of $CsPbBr_3$ on retinal development, we conducted RNA sequencing (RNA-seq) to identify gene profile changes in hEROs after three weeks of $CsPbBr_3$ and $Pb(AC)_2$ treatment. RNA was extracted from hEROs with TRIzol reagent (Invitrogen, CA, United States) and then was quantified using a NanoDrop (DE, United States) and was qualified using Agilent 2100 bioanalyzer (CA, United States). The PrimeScript RT Reagent Kit (Takara, Japan) was used to perform reverse transcription following the manufacturer's instructions and isolated using Oligo (dT)-attached magnetic beads. After reverse transcription, cDNA fragments were amplified by PCR. The expression of each gene was measured by Fragments Per Kilobase of exon per Million fragments mapped (FPKM). Genes with P-value < 0.05 and fold change > 1.2 or < 0.67 were defined as differentially expressed genes (DEGs). Kyoto Encyclopedia of Genes and Genomes (KEGG) and Gene Ontology (GO) enrichment analyses were carried out to annotate the unique biological significance and important pathways of DEGs on the Majorbio platform (https://cloud.majorbio.com). Gene Set Enrichment Analysis (GSEA) pathway analysis after $CsPbBr_3$ nanoparticles exposure was also performed using the Majorbio platform (https://cloud.majorbio.com).

Quantitative real-time PCR

To analyze the mRNA levels of the involved genes, total RNA was extracted from ten hEROs of the various groups as per the instructions of the manufacturer utilizing TRIzol reagent (15596026, Invitrogen). The total RNA of hEROs was extracted as described above and then reverse-transcribed into cDNA using the PrimeScript RT Reagent Kit (RR037A, Takara, Japan) following the manufacturer's protocol. These cDNAs were then amplified with specific gene primers (see Table S2), and quantitative real-time PCR (qRT-PCR) reactions were executed using SYBR® Premix Ex Taq™ II (Takara, Japan) with a CFX96 Real-Time PCR System (Bio-Rad, United States). The GAPDH gene was used to normalize the expression of various genes.

Statistical analysis

All results were obtained from at least three independent experiments in this study. We conducted all statistical analyses using GraphPad 8.0.432 (San Diego, CA). A One-way analysis of variance (ANOVA) followed by multiple Tukey comparisons, was used to evaluate the differences. Measurement data are presented as the mean ± SEM. Group differences between groups were considered statistically significant at: $^{*}P < 0.05$, $^{**}P < 0.01$, $^{***}P < 0.001$, and $^{****}P < 0.0001$.

Results

Synthesis and characterization of $CsPbBr_3$ and $CsPbBr_3$-SiO_2 nanoparticles

The $CsPbBr_3$ nanoparticles were synthesized using a modified supersaturated recrystallization method. A SiO_2 shell was coated on the $CsPbBr_3$ nanoparticles' surface to increase its stability and form $CsPbBr_3$-SiO_2 nanoparticles. The transmission electron microscope (TEM) images showed an average size of 30 nm for the $CsPbBr_3$ nanoparticles (Fig. S1A), with a SiO_2 thickness shell of approximately 15 nm (Fig. S1B). X-ray diffraction (XRD) patterns (Fig. S1C) confirmed that both $CsPbBr_3$ nanoparticles and $CsPbBr_3$-SiO_2 nanoparticles possessed a cubic-phased structure (PDF #18–0364), indicating that the SiO_2 shell does not alter the crystalline structure of $CsPbBr_3$ nanoparticles. Additionally, energy-dispersive X-ray spectrometry (EDS) (Fig. S1D) showed that $CsPbBr_3$-SiO_2 nanoparticles contains Cs, Pb, Br, O, and Si elements, with the fourier transform infrared (FTIR) spectra (Fig. S1E). Furthermore, X-ray photoelectron spectroscopy (XPS) detected peaks for Cs 3d, O 1s, C 1s, Pb 4f, Si 2p, and Br 3d in the $CsPbBr_3$-SiO_2 nanoparticles (Fig. S1F). The above results demonstrated the successful synthesis of $CsPbBr_3$-SiO_2 nanoparticles.

Generation and identification of hESC-derived retinal organoids

We utilized a previously published protocol from our laboratory [21, 29, 33] to culture human retina organoids. Morphological changes were captured at different time points (Days 0, 6, 18, 25, 32, and 39) (Fig. 1A). Neural retina (NR) structures in hEROs appeared around day 18 and gradually formed a lamellar structure. To evaluate the feasibility of the protocol, we stained retinal markers for day 39 hEROs. The retinal progenitor cell markers CHX10 and PAX6, retinal ganglion cell marker BRN3A, retinal anaplastic/ganglion cell marker HUC/D, and photoreceptor progenitor/precursor cell marker CRX were successfully detected in hEROs (Fig. 1B and C). CHX10-positive cells were predominantly located in the apical part of the NR, while BRN3A, PAX6, and HUC/D-positive cells were mainly distributed in the basal part of the NR (Fig. 1B and C). CRX positive cells mainly distributed in the apical-most and intermediate-deep zones of the NR (Fig. 1C). These results signify the successful establishment of our hERO model.

Influences of lead-based perovskite nanoparticles exposure on the morphogenesis of hESC-derived retinal organoids

At 18 days, the neural retina starting being formed, we initiated the $CsPbBr_3$ nanoparticles exposure while the hEROs were being cultured long-term. This exposure continued for three weeks from D18 to D39 (Fig. 1A). From days 25 to 39, we analyzed the NR structures (Fig. 2A). During the first week (Day 25), we observed

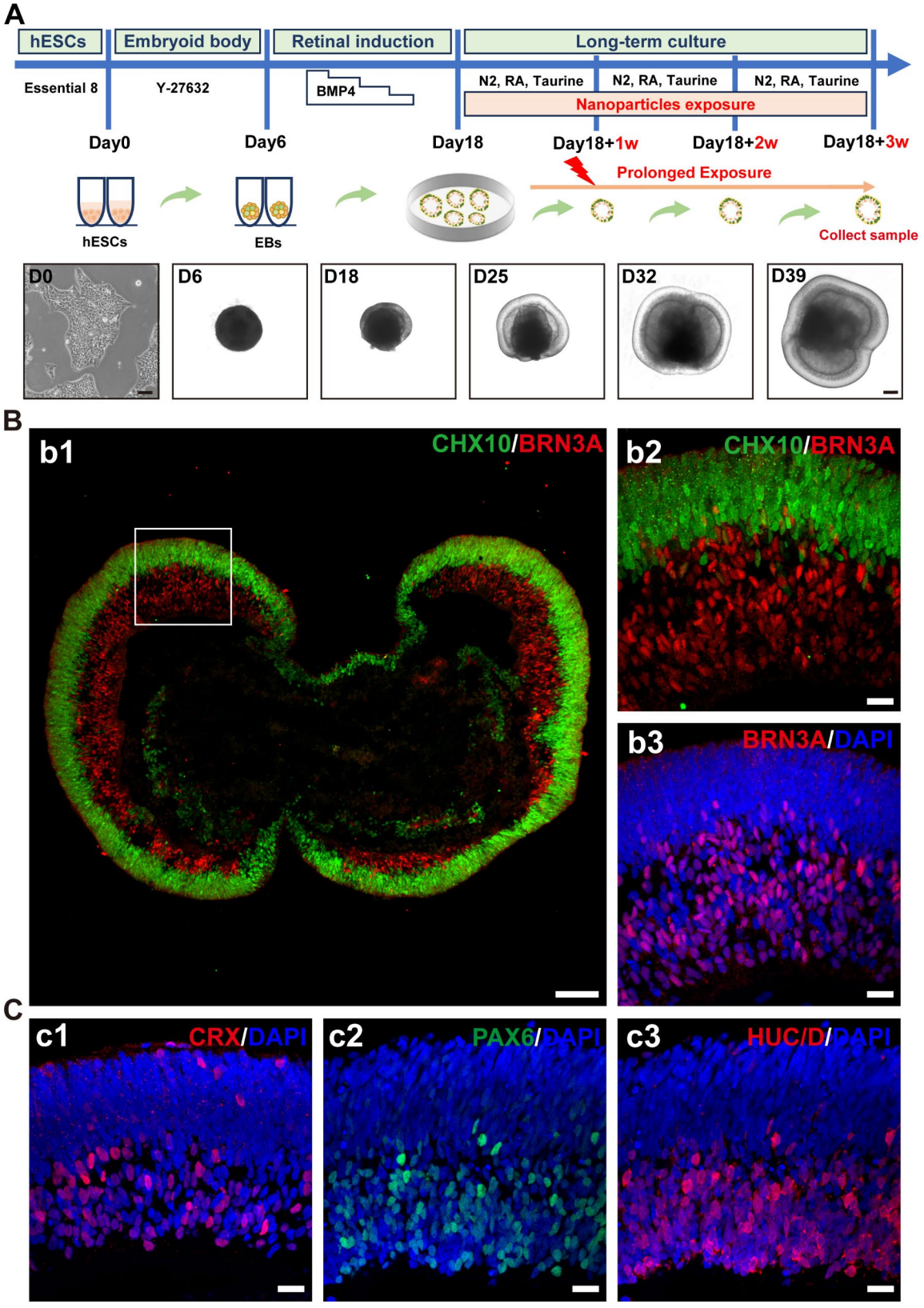

Fig. 1 Generation and identification of hESC-derived retinal organoids. (**A**) Schematic of induction and nanoparticles exposure protocols of hEROs and phase-contrast images of human retinal organoids at various differentiation days (D0, D6, D18, D25, D32, and D39). Scale bars: D0 = 100 μm, D6-D39 = 200 μm. (**B**) Immunostaining of hEROs at D39 for CHX10 and BRN3A, magnification of the white rectangle shown in b2 and b3. (**C**) c1-c3 Immunostaining of hEROs at D39 for CRX, PAX6, and HUC/D. Scale bars:100 μm(b1); 20 μm(b2-c3)

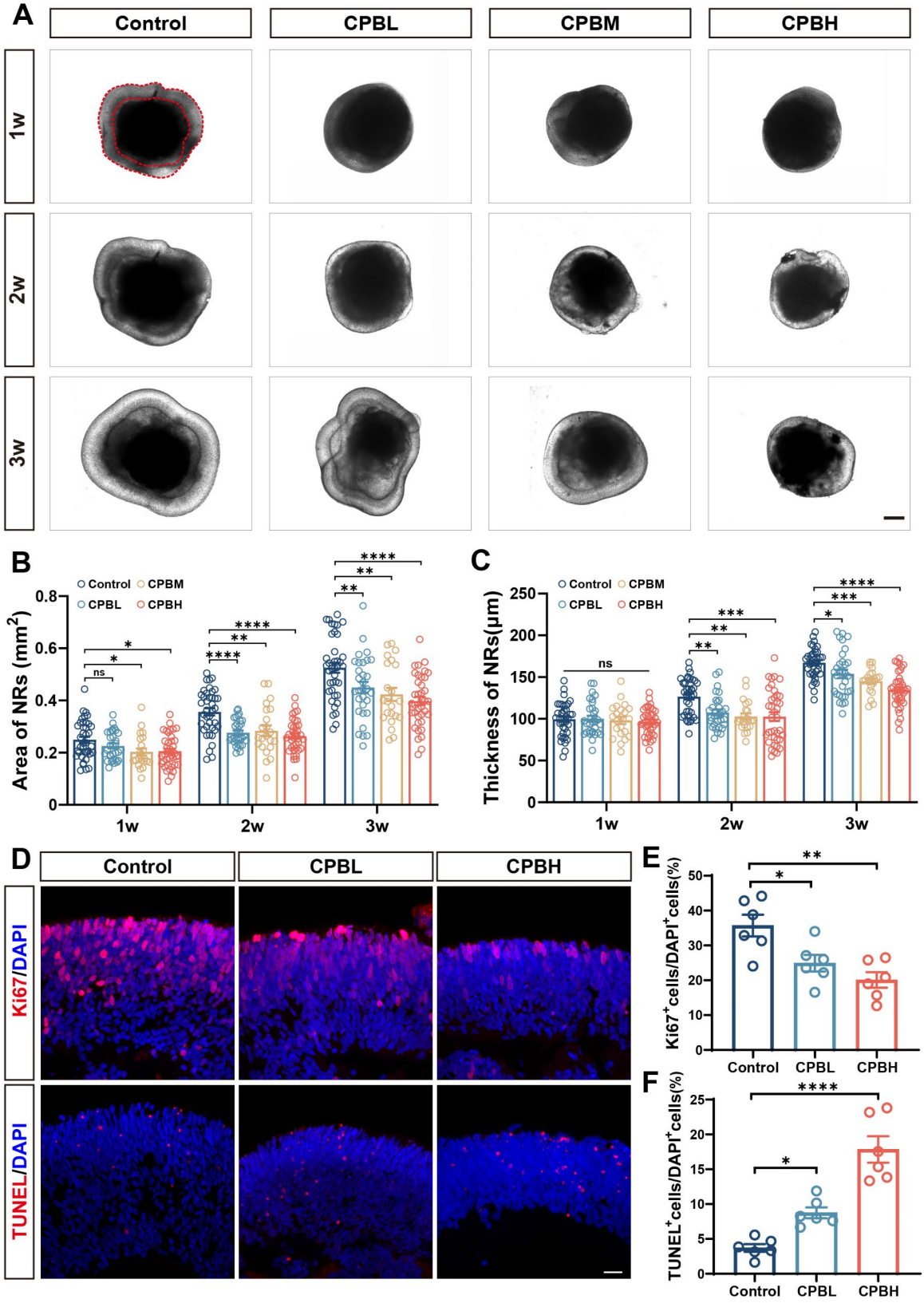

Fig. 2 (See legend on next page.)

(See figure on previous page.)

Fig. 2 Effects of $CsPbBr_3$ exposure on morphogenesis in hESC-derived retinal organoids. (**A**) Representative bright field images of hEROs at 25, 32, and 39 days after $CsPbBr_3$ exposure. Scale bars, 200 μm. (**B-C**) The area and thickness of the NRs after different concentrations of $CsPbBr_3$ exposure were calculated and statistically analyzed at 25, 32, and 39 days. Data are mean ± SEM. n: Control = 39, low-concentration $CsPbBr_3$ (CPBL) = 31, middle-concentration $CsPbBr_3$ (CPBM) = 22, high-concentration $CsPbBr_3$ (CPBH) = 38. (**D**) Representative immunohistochemical images of $Ki67^+$ and $TUNEL^+$ cells in NRs after 3w exposure to CPBL and CPBH. Scale bars, 20 μm. (**E-F**) Quantitative analysis of the proportion of $Ki67^+$ and $TUNEL^+$ cells in NRs after 3w exposure to $CsPbBr_3$. Data are mean ± SEM. $n = 6$. $^*p < 0.05$, $^{**}p < 0.01$, $^{***}p < 0.001$, $^{****}p < 0.0001$

significant differences in the area the NRs between the middle and high-concentration $CsPbBr_3$ nanoparticles groups (CPBM and CPBH) and the control group, but no significant difference in the thickness of the NRs (Fig. 2B and C). However, after two weeks of $CsPbBr_3$ nanoparticles exposure (Day 32), we noticed a significant reduction in the area and thickness of the NRs in the low-concentration $CsPbBr_3$ nanoparticles group (CPBL) compared to the control group. Additionally, after three weeks of $CsPbBr_3$ nanoparticles exposure, we observed a more pronounced reduction in the area and thickness of NRs in the CPBM and CPBH groups (Fig. 2B and C). Our results indicate a concentration-dependent reduction in the thickness and area of the NRs.

We conducted a detailed analysis of cell proliferation (Ki67) and apoptosis (TUNEL) at the hEROs level, using low and high-concentration $CsPbBr_3$ nanoparticles in present experiments. It showed a significant reduction in the proportion of Ki67-positive cells in the NRs of CPBL and CPBH when compared to the control group (Fig. 2D and E). Conversely, the proportion of TUNEL-positive cells increased significantly after three weeks of $CsPbBr_3$ nanoparticles exposure (Fig. 2D and F), with a clear concentration-dependent pattern. These findings suggest that $CsPbBr_3$ nanoparticles hinder NR cell proliferation and triggers apoptosis.

Effect of lead-based perovskite nanoparticles exposure on the retinal ganglion cell development

The first type of neuron to form in the retina during development is the retinal ganglion cells (RGCs), which are influenced by established differentiation transcription factors [34]. These cells originate from *Atoh7*-expressing transition-state progenitors and are regulated by two downstream transcription factors, *Isl1* and *Brn3*, guiding their maturation into their final phenotype. [35, 36] After exposure to $CsPbBr_3$ nanoparticles, the RGCs layers positive for ATOH7, ISL1, and BRN3A were found to be significantly thinner on day 39 (Fig. 3A), and the proportion of positive cells was correspondingly lower compared to the control group (Fig. 3B and D).

In our previous study, HUC/D, a marker for retinal anaplastic and ganglion cells, is mainly expressed within ganglion cells in retinal organoids at this stage [32]. The control group exhibited an abundant HUC/D-positive cells, while $CsPbBr_3$ nanoparticles exposure significantly reduced the proportion of HUC/D-positive cells (Fig. 3E and F). HUC/D-positive cells in the NRs of hEROs were mainly located on the basal part of the NR (Fig. 1C). Remarkably, the $CsPbBr_3$ nanoparticles exposure group had a significantly higher ratio of ectopic RGCs (RGCs that are not located in the basal part) compared to the control group (Fig. 3G). It has been previously observed that RBPMS is expressed in RGCs during the late differentiation stage [37], and our study demonstrated a significant decrease in the ratio of RBPMS-positive cells following $CsPbBr_3$ nanoparticles exposure (Fig. S3A and 3B).

Comparison of the toxic effects of $CsPbBr_3$ and $Pb(AC)_2$ and the protective effects of silica encapsulation

Previous research has found that the toxicity of $CsPbBr_3$ is predominantly caused by the production of lead ions (Pb^{2+}) during its dissolution [15, 16]. As a result, we selected lead acetate ($Pb(AC)_2$) as our positive control. Additionally, previous studies have shown that encapsulating $CsPbBr_3$ in silica can improve its stability in water [38] and potentially reduce the release of Pb^{2+}. To assess their toxicity, we exposed hEROs to three different materials at the same low preset concentrations for three weeks and recorded organoid morphology on days 25, 32, and 39 (Fig. 4A). Our findings indicate a significant decrease in area of the NRs of hEROs following one week of exposure to $Pb(AC)_2$, but not in exposure to $CsPbBr_3$ nanoparticles (Fig. 4B and C). Moreover, the area was significantly greater in the $CsPbBr_3$-SiO_2 nanoparticles group compared to the $CsPbBr_3$ nanoparticles group (Fig. 4B and C). We utilized Bio-TEM to investigate the effects of material exposure on cells (Fig. 4D). We observed intact cellular structures in the control group, including the cell membrane, nucleus, endoplasmic reticulum, mitochondria, and lysosomes (Fig. 4D). In contrast, after exposure to $CsPbBr_3$ nanoparticles, endoplasmic reticulum was swollen (Fig. 4D). Meanwhile, the nanoparticles were found in the cytoplasm and lysosomes, indicating cellular uptake of the $CsPbBr_3$ nanoparticles (Fig. 4D). Similarly, $Pb(AC)_2$ caused endoplasmic reticulum swelling but to a greater extent than that of the $CsPbBr_3$ nanoparticles group. Notably, the $CsPbBr_3$-SiO_2 nanoparticles group showed less damage compared to the $CsPbBr_3$ nanoparticles group.

Next, we obtained the dynamic distribution of the different materials in the hEROs using two-dimensional ICP-MS mapping (Fig. 5A). The results show that the

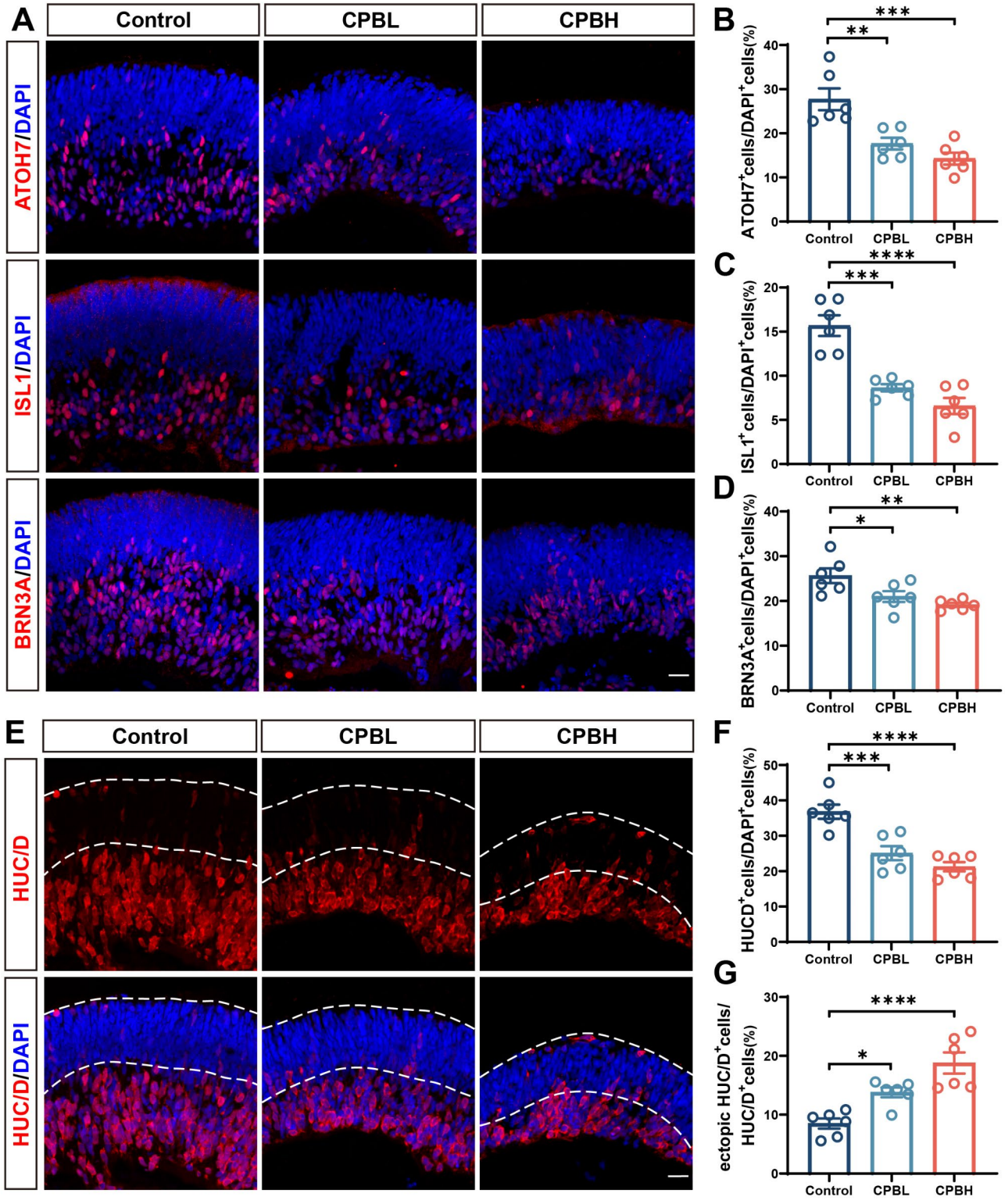

Fig. 3 Retinal ganglion cell differentiation and retinal lamination within NRs at 3w after $CsPbBr_3$ exposure. (**A**) Representative images of ATOH7$^+$, ISL1$^+$, and BRN3A$^+$ cells in the NRs. Scale bars, 20 μm. (**B-D**) Quantitation analysis for the ratio of ATOH7$^+$, ISL1$^+$, and BRN3A$^+$ cells in the NRs. Data are mean ± SEM. $n = 6$. (**E**) Representative images of HUC/D$^+$ cells in the NRs. Scale bars, 20 μm. The white line region represents the outer layer of the NRs. (**F-H**) Quantitation analysis for the ratio of HUC/D$^+$ cells and ectopic HUC/D$^+$ cells in the NRs. Data are mean ± SEM. $n = 6$. *$p < 0.05$, **$p < 0.01$, ***$p < 0.001$, ****$p < 0.0001$

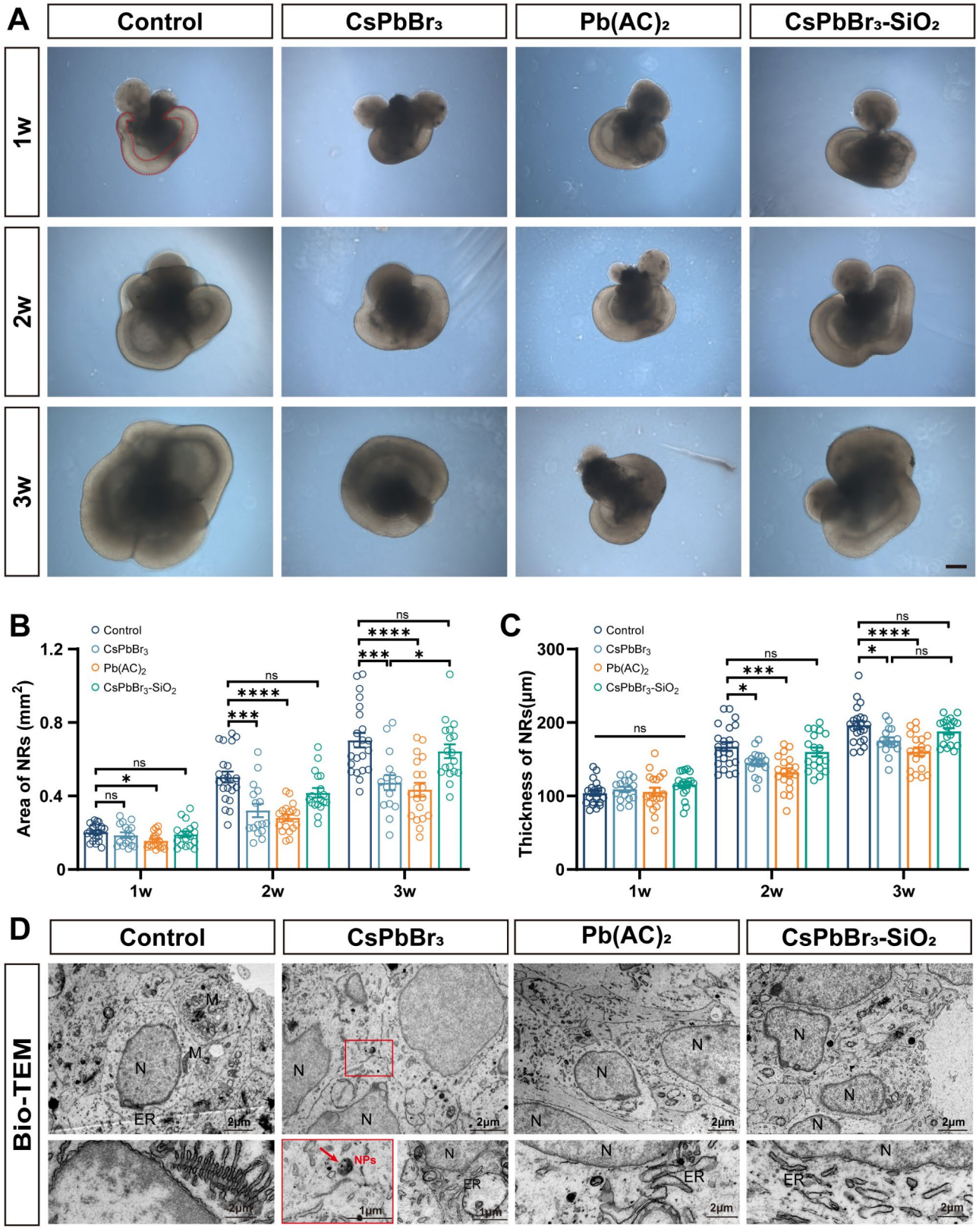

Fig. 4 Comparison of the exposure toxicity of $CsPbBr_3$ and $Pb(AC)_2$, and $CsPbBr_3$-SiO_2 exposure. (**A**) Representative bright field images of hEROs at 25, 32, and 39 days after materials exposure (The NR layer: red annule region). Scale bar, 250 μm. (**B-C**) The area and thickness of the NRs after materials exposure were calculated and statistically analyzed at 39 days. Data are mean ± SEM. n: Control = 22, $CsPbBr_3$ = 16, $Pb(AC)_2$= 19, $CsPbBr_3$ -SiO_2 = 18. (**D**) Bio-TEM images of NRs (nanoparticles: red arrow). N, nucleus; ER, endoplasmic reticulum; and NPs, nanoparticles. *$p < 0.05$, ***$p < 0.001$, ****$p < 0.0001$

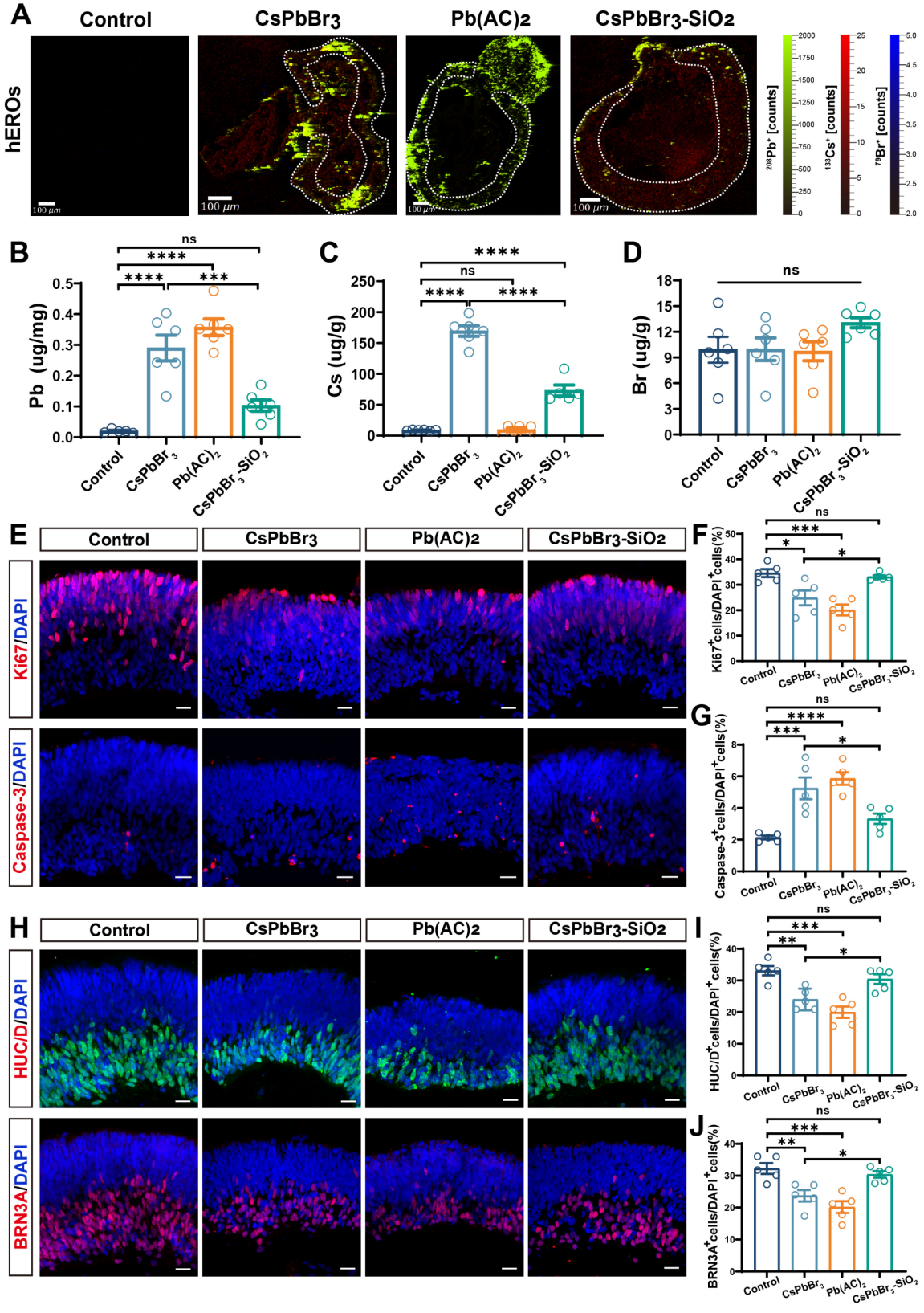

Fig. 5 (See legend on next page.)

(See figure on previous page.)

Fig. 5 The material distribution, accumulation, and development effects of $CsPbBr_3$, $Pb(AC)_2$, and $CsPbBr_3$-SiO_2 exposure. (**A**) Distribution detection of Pb, Cs, and Br in hEROs (The NR layer: white annule region). (**B-D**) Quantitative analysis of Pb, Cs, and Br enrichment in hEROs by ICP-MS, $n \geq 5$. Data are mean ± SEM. (**E** and **H**) Representative images of Ki67, Caspase-3, HUC/D, and BRN3A positive cells in the NRs. Scale bars, 20 μm. (**F-G** and **I-J**) Quantitation analysis for the ratio of Ki67, Caspase-3, HUC/D, and BRN3A positive cells in the NRs. Data are mean ± SEM. $n = 5$. $^{*}p < 0.05$, $^{**}p < 0.01$, $^{***}p < 0.001$, $^{****}p < 0.0001$

NR layers of the $CsPbBr_3$ nanoparticles group tend to have uniformly distributed Pb, Br, and Cs elements. Similarly, the distribution of elements in the $Pb(AC)_2$ and $CsPbBr_3$-SiO_2 groups was also uniform (Fig. 5A). To further investigate the amount of material accumulated in the organoids, we employed ICP-MS to analyze the Pb, Cs, and Br content in the hEROs. Our findings revealed that the $Pb(AC)_2$ group contained a higher lead content than the $CsPbBr_3$ nanoparticle group. Both groups feature significantly higher lead content when compared to the control group (Fig. 5B). Interestingly, we observed a significant decrease in both Pb and Cs content in the $CsPbBr_3$-SiO_2 nanoparticles group when compared to the $CsPbBr_3$ group (Fig. 5B and C). However, no significant difference in Br content was observed among the groups (Fig. 5D). We suspect that lead uptake by the hEROs is the primary reason for the observed morphological differences.

We proceeded to assess the cell proliferation and apoptosis of the NRs (Fig. 5E). Our findings indicate that the proportion of proliferating cells in NRs was significantly lower in the $CsPbBr_3$ nanoparticles and $Pb(AC)_2$ groups compared to the control group (Fig. 5F). A noteworthy observation was that the ratio of Ki67-positive cells in the $CsPbBr_3$-SiO_2 nanoparticles group was higher than that in the $CsPbBr_3$ nanoparticles group (Fig. 5F). Conversely, the ratio of Caspase-3-positive cells in the $CsPbBr_3$-SiO_2 nanoparticles group was lower than that in the $CsPbBr_3$ nanoparticles group (Fig. 5G). We also evaluated the development of RGCs using representative markers of HUC/D and BRN3A for immunohistochemical staining (Fig. 5H). Our results indicate a significant reduction in the ratio of RGCs in the $CsPbBr_3$ nanoparticles and $Pb(AC)_2$ groups compared to the control (Fig. 5I and J). On the other hand, the ratio of RGCs in the $CsPbBr_3$-SiO_2 nanoparticles group showed no significant difference compared to the control group, while was increased when compared to the $CsPbBr_3$ nanoparticles group (Fig. 5I and J). We also found a tendency of the percentage of RGCs in the $Pb(AC)_2$ group than in the $CsPbBr_3$ nanoparticles group, although the difference was insignificant (Fig. 5I and J). Our observations led us to believe that the same mass concentration of $Pb(AC)_2$ has a more substantial impact on the early development of retinal progenitor cells than that of $CsPbBr_3$ due to the hEROs taking in a higher lead concentration in the $Pb(AC)_2$ group compared to the $CsPbBr_3$ nanoparticles group. Notably, silica coating of $CsPbBr_3$ nanoparticles reduced the retinal early developmental toxicity of $CsPbBr_3$ nanoparticles to some extent.

Exploration of the molecular mechanisms underlying the effects of $CsPbBr_3$ exposure on hESC-derived retinal organoids

We utilized transcriptome sequencing to uncover the molecular mechanisms underlying the effects of exposure to $CsPbBr_3$ nanoparticles on early retinal development. The gene expression profiles of the $CsPbBr_3$ and $Pb(AC)_2$ groups, at low concentration, were compared to the control group using cluster analysis and plotted on a heat map (Fig. S4A-S4B). Our study revealed 2780 differentially expressed genes (DEGs) in the $CsPbBr_3$ group, with 1626 up-regulated and 1154 down-regulated genes (Fig. 6A). A Venn diagram indicated that 1455 DEGs were common to both the $CsPbBr_3$ and $Pb(AC)_2$ groups (Fig. 6B). KEGG enrichment analysis of the DEGs in the $CsPbBr_3$ group identified significant enrichment in signaling pathways regulating pluripotency of stem cells and calcium signaling pathways (Fig. 6C). Similar enrichment pathways were observed in the $Pb(AC)_2$ group (Fig. S4C). GSEA analysis also revealed significant enrichment of the calcium signaling pathway in the $CsPbBr_3$ group (Fig. 6D). We performed a clustered heat map analysis of differential genes corresponding to the calcium signaling pathway. We observed differential upregulation of the RYR2 and ITPR1 pathways and differential downregulation of ATP2A3 and HRC on the endoplasmic reticulum (Fig. 6E).

The endoplasmic reticulum (ER) is vital in maintaining intracellular calcium homeostasis [39] through a variety of calcium channels, including RYR2 and ITPR1, which release calcium [40], and the Ca^{2+} ATPase pump (SERC) encoded by the ATP2A1-3 gene, responsible for transporting calcium ions from the cytoplasm into the ER [41]. Additionally, HRC buffers calcium in the ER [42]. However, when these channels become dysregulated, with RYR2 and ITPR1 being up regulated while ATP2A3 and HRC being down-regulated, excessive calcium is released, disrupting the balance and causing calcium depletion. Previous studies have linked endoplasmic reticulum calcium depletion to ER stress, triggering the unfolded protein response [43, 44], ultimately leading to apoptosis [45–47]. RT-PCR was performed to detect the expression levels of calcium channel-related genes, including ITPR1, RYR2, ATP2A3, and HRC mRNA (Fig. 7A-D). The results showed that endoplasmic reticulum calcium release

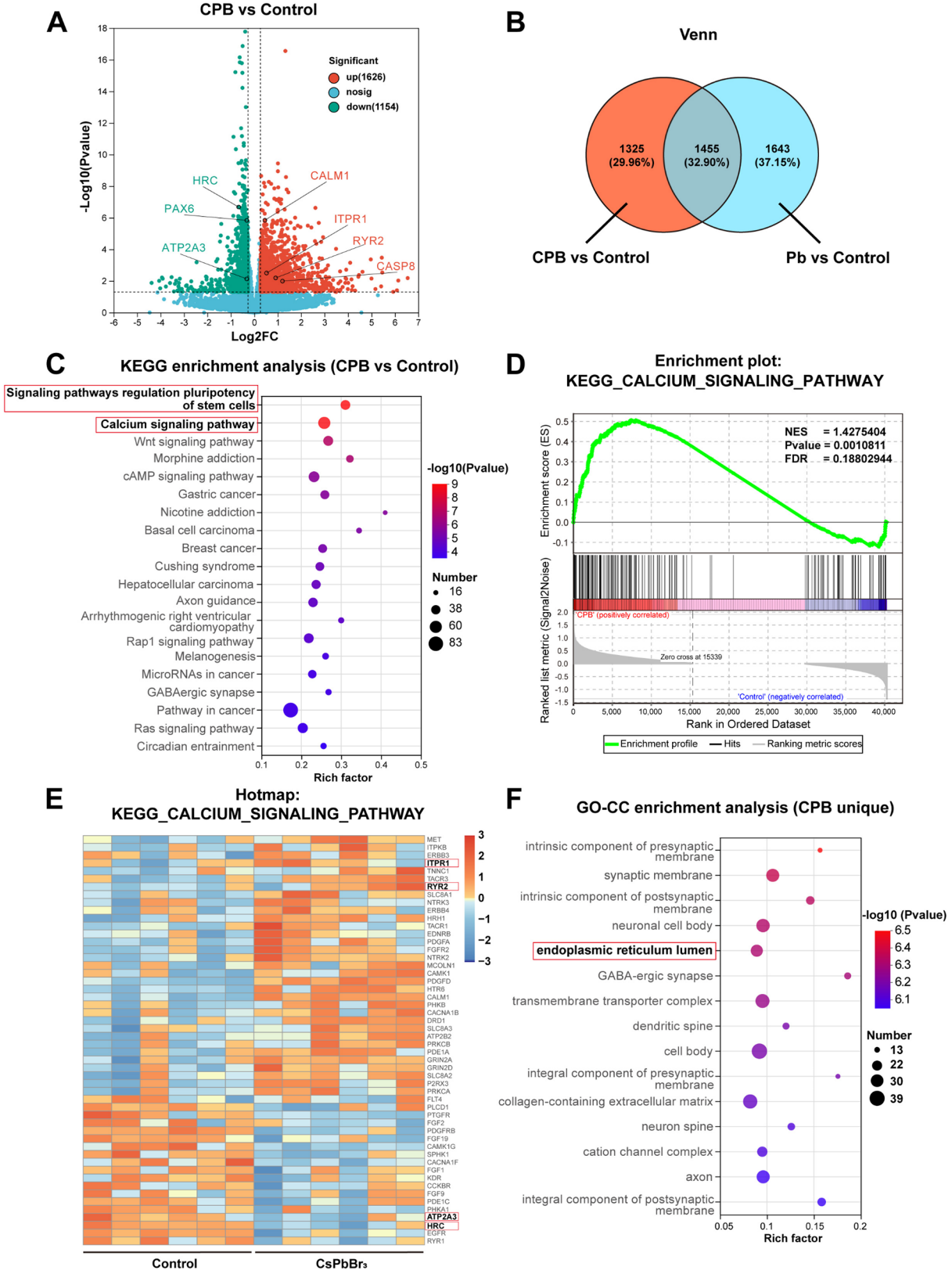

Fig. 6 (See legend on next page.)

(See figure on previous page.)

Fig. 6 Transcriptomic analysis of 39 days hEROs after 3 weeks of $CsPbBr_3$ exposure. (**A**) Volcano plots of DEGs in the $CsPbBr_3$ nanoparticles (CPB) group vs. control group. (**B**) Venn plots of DEGs in the $CsPbBr_3$ nanoparticles (CPB) and $Pb(AC)_2$ groups (Pb) compared to the control group. (**C**) $CsPbBr_3$ nanoparticles group differential gene KEGG-enriched TOP20 pathway. (**D**) GSEA analysis of the enriched calcium signaling pathway graph. (**E**) Heatmap of differential expression of selected genes in the calcium signaling pathway enriched with KEEG. (**F**) Bubble plots of cellular components in the GO enrichment analysis of differentially expressed genes specific to the $CsPbBr_3$ nanoparticles (CPB) group

channel-related genes ITPR1 and RYR2 were significantly up-regulated, while calcium stabilizing protein-related genes and calcium influx channel-related genes HRC and ATP2A3 were significantly down-regulated, indicating the occurrence of endoplasmic reticulum stress. To better understand the unique mechanisms involved in exposure to $CsPbBr_3$ nanoparticles, we conducted a GO enrichment analysis of the 1325 differential genes specific to this group. The GO-CC data revealed significant enrichment of the endoplasmic reticulum lumen (Fig. 6F), indicating that exposure to $CsPbBr_3$ nanoparticles altered the endoplasmic reticulum of cells. Bio-TEM analysis of NR cells confirmed that $CsPbBr_3$ nanoparticles could enter cells and cause swelling in the endoplasmic reticulum, with more severe damage observed in the $Pb(AC)_2$ group and less severe damage in the $CsPbBr_3$-SiO_2 group (Fig. 4D). These findings provide further evidence of the toxicity mechanism of $CsPbBr_3$ nanoparticles exposure and the protective effect of encapsulated silica.

The research has confirmed that excessive endoplasmic reticulum stress leads to abnormalities in neurogenesis [48]. A previous study found that endoplasmic reticulum stress can decrease *PAX6* mRNA levels, disrupting normal neural development [49]. *PAX6* is crucial in retinal development [50] as it triggers the bHLH transcription factor *ATOH7*, which regulates downstream *ISL1* and *BRN3* genes necessary for retinal ganglion cell differentiation [51]. RNA-seq data indicated that the *PAX6* gene, which is responsible for regulating the stem cell pluripotency pathway, was significantly down-regulated after $CsPbBr_3$ nanoparticles treatment (Fig. 6A). RT-PCR results also showed a significant reduction in the expression of *PAX6* in the $CsPbBr_3$ nanoparticles and $Pb(AC)_2$ exposure group(Fig. 7E). In addition, immunofluorescence staining revealed a notable decrease in the percentage of PAX6-positive cells (Fig. 7F and G).

Discussion

In this study, we analyzed the effects of $CsPbBr_3$ nanoparticles exposure on early retinal development utilizing human embryonic stem cell-derived retinal organoids. We found that $CsPbBr_3$ nanoparticles exposure inhibited cell proliferation and promoted apoptosis of the NRs, ultimately reducing in the area and thickness of the NRs. RGCs are the first cell type to emerge during retinal development, and our immunofluorescence analysis demonstrated that $CsPbBr_3$ nanoparticles exposure results in abnormal early RGC development, with a decrease in their percentage in the NRs and an increase in ectopic RGCs. Further, we combined RNA-seq analysis and found that $CsPbBr_3$ nanoparticles exposure disrupted calcium signaling pathways in the endoplasmic reticulum, which led to endoplasmic reticulum calcium depletion and the development of endoplasmic reticulum stress.

hEROs reproduce the main structural features of early retinal development [25]. Retinal organoids contain predominantly retinal cell subtypes and have hierarchical structures that resemble in vivo morphology [25, 52]. Retinal organoids offer many advantageous, such as the ability to screen of drugs on a large scale, model retinal diseases in vitro, and potentially treat ocular diseases [53–55]. In addition, retinal organoids are a reliable tool for toxicological assessment, with effects similar to those observed in humans and other in vivo models [26]. Given the superiority of this model, we utilized it to assess the early retinal developmental toxicity of $CsPbBr_3$ nanoparticles. As far as we know, this is the first study to report on the neurotoxicity and molecular mechanisms of $CsPbBr_3$ nanoparticles exposure during this critical stage of retinal development.

Previous studies have shown that $CsPbBr_3$ nanoparticles exposure can cause damage to the nervous system, circulatory system, respiratory system, and digestive system [5, 23, 24, 57]. Animal experiments showed that learning, memory, and cognitive functions were adversely affected in C57BL/6J mice exposed to 25 mg/kg of $CsPbBr_3$ nanoparticles every other day for 28 days via nasal drip [56]. In an acute exposure experiment involving zebrafish larvae, they were exposed for 96 h to different lead-based perovskite solutions with an LD50 of around 212 μg/mL (Pb^{2+} concentration at 71 μg/mL) [16]. Most studies have concluded that Pb^{2+} release primary contributes to the toxicity associated with $CsPbBr_3$ nanoparticle exposure [3, 16]. Lead is widely known as a neurotoxic substance [58]. Moreover, lead ions can readily cross the placental barrier, potentially disrupting the normal development of the fetus [59]. Therefore, it is necessary to evaluate the effect of $CsPbBr_3$ nanoparticles on human retinal development. It was found that exposure of C57BL/6N mice to 55 ppm lead acetate drinking water during pregnancy resulted in delayed differentiation of optic rod cells [60]. Compared to the control group, the differentiation of retinal ganglion cells was not affected [60]. Earlier studies have also found that developmental lead exposure in monkeys or rats selectively

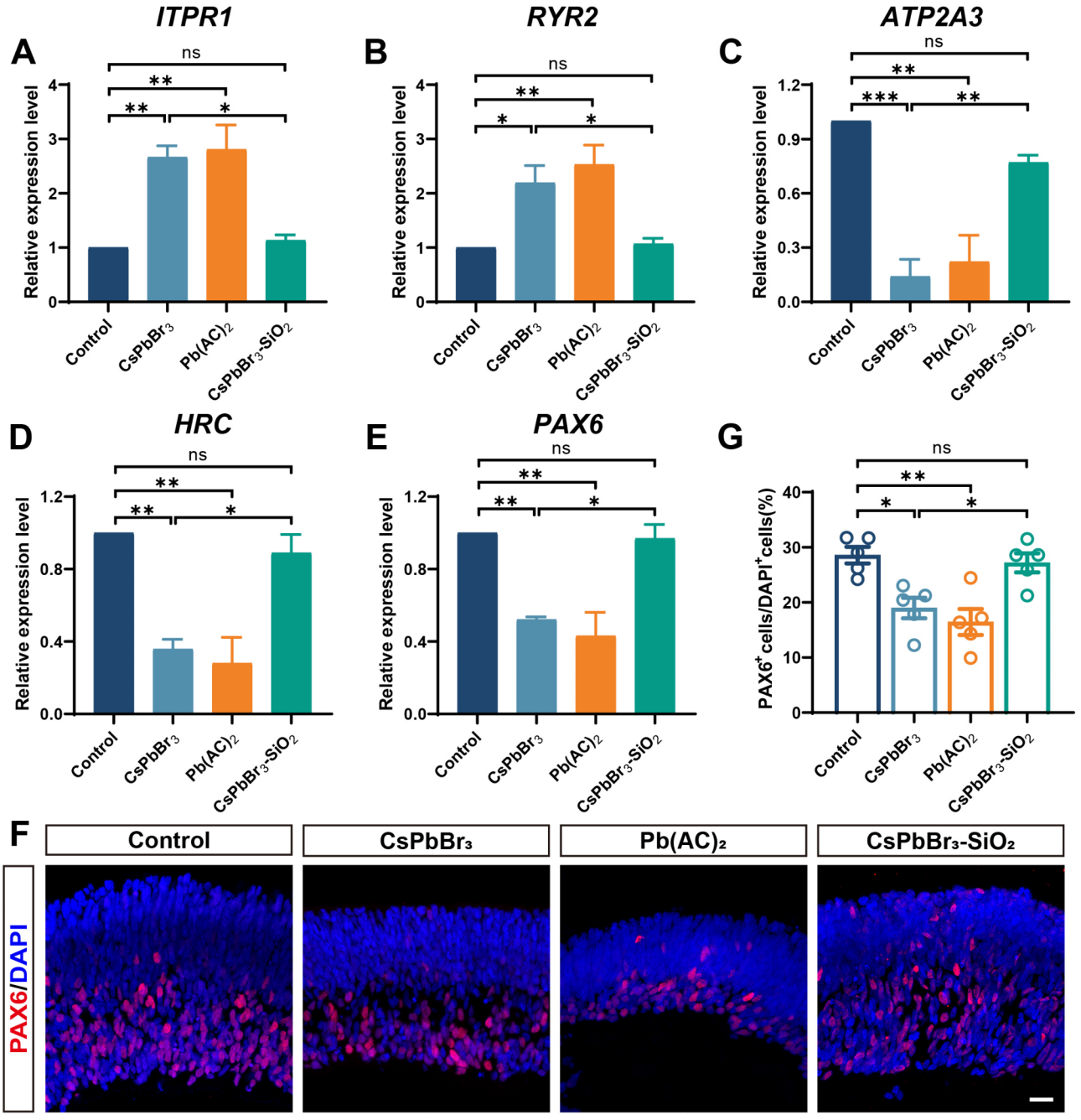

Fig. 7 Materials exposure leads to changes in endoplasmic reticulum calcium channels and inhibits PAX6 expression. (**A-E**) Comparison of the expression levels of *ITPR1*, *RYR2*, *ATP2A3*, and *HRC* mRNA and *PAX6* mRNA between control and exposed groups. Data are mean ± SEM. $n = 3$. (**F**) Representative images of PAX6$^+$ cells in the NRs. Scale bars, 20 μm. (**G**) Quantitation analysis for the ratio of PAX6$^+$ cells in the NRs. Data are mean ± SEM. $n = 5$. $^*p < 0.05$, $^{**}p < 0.01$, $^{***}p < 0.001$

induces abnormalities in optic rod cells [61]. However, the present study found that $CsPbBr_3$ nanoparticles exposure leads to a reduction in the thinning of the NRs in retinal organoids and a reduction in the ratio of RGCs. In addition, the ratio of ectopic RGCs was significantly increased after $CsPbBr_3$ nanoparticles exposure. The distribution of RGCs in the correct location is a critical first step in forming other retinal layers, and ectopic ganglion cells will induce layering defects in the developing retina [62]. Retinal lamination is an important step in unique retinal morphogenesis, and alterations in this process may impair visual function [63, 64]. We also found that retinal progenitor cells located in the outer layer of the NRs also had a significantly less cellular proportion after

$CsPbBr_3$ nanoparticles exposure (Figure S6). In general, $CsPbBr_3$ nanoparticles exposure severely affected the differentiation of retinal ganglion cells in organoids.

We also utilized $Pb(AC)_2$ as a positive control at the same mass concentration. We found that the $Pb(AC)_2$ group resulted in a thinner neural layer and a slight decrease in the ratio of RGCs than the $CsPbBr_3$ nanoparticles group. Combined with ICP-MS analysis, we found that the amount of lead accumulated in hEROs was slightly higher in the $Pb(AC)_2$ group than in the $CsPbBr_3$ nanoparticles group. This may explain why the effect of $Pb(AC)_2$ on the development of hEROs at the same mass concentration was more pronounced than the $CsPbBr_3$ nanoparticles group. This is consistent with previous studies in which $CsPbBr_3$ nanoparticles toxicity was attributed to released lead.

Mesoporous silicas are broadly used in the biomedical fields due to their mesoporous structure, high specific surface area, and exceptional biocompatibility [65, 66]. Previous studies demonstrated that silica coatings on the surface of ZnO nanoparticles can significantly reduce the release of zinc ions from the dissolution of core ZnO nanoparticles, potentially alleviating toxicity [67, 68]. It has also been found that mesoporous silica nanoparticles encapsulating perovskite nanoparticles improve stability [38]. Therefore, in the present work, the toxicity was also reduced through mesoporous silica encapsulation. ICP-MS analysis revealed that the lead concentration in the hEROs following mesoporous silica encapsulation was significantly lower than in the $CsPbBr_3$ nanoparticle group. Then, immunohistochemical analysis revealed that the silica encapsulation method could reduce the effects of $CsPbBr_3$ nanoparticles exposure. This suggests that mesoporous silica encapsulation of $CsPbBr_3$ nanoparticles may be feasible to reduce toxicity. However, this method needs to be further investigated industrially to minimize the effect on the physicochemical properties of $CsPbBr_3$ itself.

We further explored the potential mechanisms of early retinal developmental abnormalities induced by $CsPbBr_3$ nanoparticles exposure using RNA-Seq. Based on KEGG enrichment analysis, the calcium signaling pathway was significantly associated with $CsPbBr_3$ nanoparticles exposure. Previous research has shown that the calcium signaling pathway is crucial in neural induction and differentiation [69]. In our RNA sequencing efforts, significant changes were found in calcium channels in the endoplasmic reticulum, including up-regulated *ITPR1*, *RYR2*, and down-regulated *ATP2A3*, *HRC*. Disruption of these channels leads to endoplasmic reticulum calcium depletion, eventually inducing endoplasmic reticulum stress [43, 70]. It was found that significant endoplasmic reticulum stress and oxidative stress occur in zebrafish fertilized eggs exposed to low levels of lead for 48 h and can lead to subsequent developmental abnormalities in zebrafish embryos [71]. Endoplasmic reticulum stress is also pivotal in ganglion cell death in eye diseases [72–74]. Therefore, we speculated that endoplasmic reticulum stress also plays an important role in the developmental abnormalities of retinal ganglion cells caused by $CsPbBr_3$ nanoparticles exposure. However, more in-depth studies are needed to explore the developmental toxicity of $CsPbBr_3$ nanoparticles exposure.

Conclusion

In conclusion, this study used a three-dimensional floating retinal organoid model to reveal the effects of $CsPbBr_3$ nanoparticles exposure on early human retinal development. Our results suggest that retinal organoids are reliable for assessing nanomaterial developmental toxicity. Firstly, $CsPbBr_3$ nanoparticles affect the proliferation and differentiation of retinal progenitor cells. Secondly, $CsPbBr_3$ nanoparticles are less toxic than conventional soluble $Pb(AC)_2$, which can release more Pb^{2+} into the organoid and result in toxicity. Then, we initially found that mesoporous silica encapsulation of $CsPbBr_3$ nanoparticles is a feasible method to reduce the toxicity of $CsPbBr_3$ nanoparticles, yet more studies are still needed to optimize this method. In addition, transcriptomic analysis revealed that endoplasmic reticulum calcium homeostasis disorders and regulation of stem cell pluripotency are related to $CsPbBr_3$ nanoparticles-induced early retinal developmental toxicity.

Supplementary Information

The online version contains supplementary material available at https://doi.org/10.1186/s12951-025-03245-w.

Supplementary Material 1: More details on characterization of nanoparticles, actual concentration of the culture medium, cluster heat map analysis of $CsPbBr_3$ and $Pb(AC)_2$ exposure groups and the KEGG analysis of $Pb(AC)_2$ exposure groups, and information of primary antibodies and primers used in this study.

Acknowledgements
Not applicable.

Author contributions
C.Y. and Z. D. contributed equally to this work. C.Y., Z. D.: Conceptualization; Data curation; Formal analysis; Investigation; Methodology; Writing - Original Draft. L. M., X. C., Y. L., L. G., J. K.: Formal analysis; Investigation; Methodology; Software; Visualization. Z. G.: Supervision; Writing - review & editing. X. F.: Supervision; Funding acquisition; Writing - review & editing. H. X.: Project administration; Resources; Funding acquisition; Supervision; Writing - review & editing. All authors read and approved the final manuscript.

Funding
This study was supported by funding from the National Key Research and Development Program of China (Grant No. 2021YFA1101203, 2024YFA1108702).

Data availability
No datasets were generated or analysed during the current study.

Declarations

Ethics approval and consent to participate
Not applicable.

Consent for publication
Not applicable.

Competing interests
The authors declare no competing interests.

Author details
[1]Southwest Eye Hospital, Southwest Hospital, Third Military Medical University (Army Medical University), Chongqing 400038, China
[2]Key Lab of Visual Damage and Regeneration & Restoration of Chongqing, Southwest Eye Hospital, Southwest Hospital, Chongqing 400038, China
[3]Key Laboratory of Extreme Environmental Medicine Ministry of Education, Department of Military Cognitive Psychology, School of Psychology, Third Military Medical University (Army Medical University), Chongqing 400038, China
[4]Institute of High Energy Physics and National Center for Nanoscience and Technology, CAS Key Laboratory for Biomedical Effects of Nanomaterials and Nanosafety and CAS Center for Excellence in Nanoscience, Chinese Academy of Sciences, Beijing 100049, China
[5]College of Materials Science and Optoelectronic Technology, University of Chinese Academy of Sciences, Beijing 100049, China

Received: 23 June 2024 / Accepted: 18 February 2025
Published online: 26 February 2025

References

1. Lee MM, Teuscher J, Miyasaka T, et al. Efficient hybrid solar cells based on meso-superstructured organometal halide perovskites. Science. 2012;338(6107):643–7. https://doi.org/10.1126/science.1228604. [published Online First: 2012/10/09].
2. Fu P, Shan Q, Shang Y, et al. Perovskite nanocrystals: synthesis, properties and applications. Sci Bull (Beijing). 2017;62(5):369–80. https://doi.org/10.1016/j.scib.2017.01.006. [published Online First: 2017/03/01].
3. Ren M, Qian X, Chen Y, et al. Potential lead toxicity and leakage issues on lead halide perovskite photovoltaics. J Hazard Mater. 2022;426:127848. https://doi.org/10.1016/j.jhazmat.2021.127848. [published Online First: 2021/11/29].
4. Chen Y, Liu X, Wang T, et al. Highly stable inorganic lead halide perovskite toward efficient photovoltaics. Acc Chem Res. 2021;54(17):3452–61. https://doi.org/10.1021/acs.accounts.1c00343. [published Online First: 2021/08/25].
5. Guo J, Lu M, Zhang X, et al. Highly stable and efficient Light-Emitting diodes based on orthorhombic γ-CsPbI(3) nanocrystals. ACS Nano. 2023;17(10):9290–301. https://doi.org/10.1021/acsnano.3c00789. [published Online First: 2023/05/01].
6. Wang S, Li L, Weng W, et al. Trilayered lead chloride perovskite ferroelectric affording Self-Powered Visible-Blind ultraviolet photodetection with large Zero-Bias photocurrent. J Am Chem Soc. 2020;142(1):55–9. https://doi.org/10.1021/jacs.9b10919. [published Online First: 2019/12/17].
7. Wu X, Guo Z, Zhu S, et al. Ultrathin, transparent, and high density perovskite scintillator film for high resolution X-Ray microscopic imaging. *Advanced science (Weinheim*. Baden-Wurttemberg Germany). 2022;9(17):e2200831. https://doi.org/10.1002/advs.202200831. [published Online First: 2022/04/29].
8. Yan F, Tan ST, Li X, et al. Light generation in lead halide perovskite nanocrystals: leds, color converters, lasers, and other applications. Small. 2019;15(47):e1902079. https://doi.org/10.1002/smll.201902079. [published Online First: 2019/10/28].
9. Yuan C, Li X, Semin S, et al. Chiral lead halide perovskite nanowires for Second-Order nonlinear optics. Nano Lett. 2018;18(9):5411–17. https://doi.org/10.1021/acs.nanolett.8b01616. [published Online First: 2018/08/14].
10. Ravi VK, Mondal B, Nawale VV, et al. Don't let the lead out: new material chemistry approaches for sustainable lead halide perovskite solar cells. ACS Omega. 2020;5(46):29631–41. https://doi.org/10.1021/acsomega.0c04599. [published Online First: 2020/12/01].
11. Zhuang J, Wang J, Yan F. Review on chemical stability of lead halide perovskite solar cells. Nanomicro Lett. 2023;15(1):84. https://doi.org/10.1007/s40820-023-01046-0. [published Online First: 2023/04/01].
12. Schmidt F, Ledermann L, Schäffer A, et al. Rapid sequestration of perovskite solar cell-derived lead in soil. J Hazard Mater. 2022;436:128995. https://doi.org/10.1016/j.jhazmat.2022.128995. [published Online First: 2022/05/08].
13. Mallick A, Mendez Lopez RD, Arye G, et al. Soil adsorption and transport of lead in the presence of perovskite solar cell-derived organic cations. J Hazard Mater. 2023;451:131147. https://doi.org/10.1016/j.jhazmat.2023.131147. [published Online First: 2023/03/10].
14. Khalifa SA, Spatari S, Fafarman AT, et al. Fate and exposure assessment of Pb leachate from hypothetical breakage events of perovskite photovoltaic modules. Environ Sci Technol. 2023;57(13):5190–202. https://doi.org/10.1021/acs.est.2c05815.
15. Kwak JI, Kim L, An YJ. Sublethal toxicity of PbI(2) in perovskite solar cells to fish embryos (Danio rerio and Oryzias latipes): deformity and growth Inhibition. Sci Total Environ. 2021;771:145388. https://doi.org/10.1016/j.scitotenv.2021.145388. [published Online First: 2021/02/06].
16. Patsiou D, Del Rio-Cubilledo C, Catarino AI, et al. Exposure to Pb-halide perovskite nanoparticles can deliver bioavailable Pb but does not alter endogenous gut microbiota in zebrafish. Sci Total Environ. 2020;715:136941. https://doi.org/10.1016/j.scitotenv.2020.136941. [published Online First: 2020/02/12].
17. Wu X, Cobbina SJ, Mao G, et al. A review of toxicity and mechanisms of individual and mixtures of heavy metals in the environment. Environ Sci Pollut Res Int. 2016;23(9):8244–59. https://doi.org/10.1007/s11356-016-6333-x. [published Online First: 2016/03/12].
18. Goyer RA. Transplacental transport of lead. Environ Health Perspect. 1990;89:101–5. https://doi.org/10.1289/ehp.9089101. [published Online First: 1990/11/01].
19. Rothenberg SJ, Schnaas L, Salgado-Valladares M, et al. Increased ERG a- and b-wave amplitudes in 7- to 10-year-old children resulting from prenatal lead exposure. Investig Ophthalmol Vis Sci. 2002;43(6):2036–44. [published Online First: 2002/05/31].
20. London A, Benhar I, Schwartz M. The retina as a window to the brain-from eye research to CNS disorders. Nat Rev Neurol. 2013;9(1):44–53. https://doi.org/10.1038/nrneurol.2012.227. [published Online First: 2012/11/21].
21. Li M, Zeng Y, Ge L, et al. Evaluation of the influences of low dose polybrominated Diphenyl ethers exposure on human early retinal development. Environ Int. 2022;163:107187. https://doi.org/10.1016/j.envint.2022.107187. [published Online First: 2022/03/22].
22. Fox DA. Retinal and visual system: occupational and environmental toxicology. Handb Clin Neurol. 2015;131:325–40. https://doi.org/10.1016/b978-0-444-62627-1.00017-2. [published Online First: 2015/11/14].
23. Mei L, Guo J, He R, et al. CsPbBr(3) perovskite nanoparticles causes Colitis-Like symptom via promoting intestinal barrier damage and gut microbiota dysbiosis. Small. 2023;19(32):e2301129. https://doi.org/10.1002/smll.202301129. [published Online First: 2023/04/19].
24. Ding X, He R, Zhang T, et al. Lung toxicity and molecular mechanisms of Lead-Based perovskite nanoparticles in the respiratory system. ACS Appl Mater Interfaces. 2023;15(36):42139–52. https://doi.org/10.1021/acsami.3c04255. [published Online First: 2023/08/31].
25. O'Hara-Wright M, Gonzalez-Cordero A. Retinal organoids: a window into human retinal development. Development. 2020;147(24). https://doi.org/10.1242/dev.189746. [published Online First: 2020/12/29].
26. Dorgau B, Georgiou M, Chaudhary A, et al. Human retinal organoids provide a suitable tool for toxicological investigations: A comprehensive validation using drugs and compounds affecting the retina. Stem Cells Transl Med. 2022;11(2):159–77. https://doi.org/10.1093/stcltm/szab010. [published Online First: 2022/03/18].
27. Baek A, Kwon IH, Lee DH, et al. Novel organoid culture system for improved safety assessment of nanomaterials. Nano Lett. 2024;24(3):805–13. https://doi.org/10.1021/acs.nanolett.3c02939. [published Online First: 2024/01/12].
28. Kuwahara A, Ozone C, Nakano T, et al. Generation of a ciliary margin-like stem cell niche from self-organizing human retinal tissue. Nat Commun. 2015;6:6286. https://doi.org/10.1038/ncomms7286. [published Online First: 2015/02/20].
29. Zou T, Gao L, Zeng Y, et al. Organoid-derived C-Kit(+)/SSEA4(-) human retinal progenitor cells promote a protective retinal microenvironment during transplantation in rodents. Nat Commun. 2019;10(1):1205. https://doi.org/10.1038/s41467-019-08961-0. [published Online First: 2019/03/16].

30. Mahdi AA, Ansari JA, Chaurasia P, et al. A study of maternal and umbilical cord blood lead levels in pregnant women. Indian J Clin Biochem. 2023;38(1):94–101. https://doi.org/10.1007/s12291-022-01040-0. [published Online First: 2023/01/24].
31. Charkiewicz AE, Backstrand JR. Lead toxicity and pollution in Poland. Int J Environ Res Public Health. 2020;17(12). https://doi.org/10.3390/ijerph17124385. [published Online First: 2020/06/24].
32. Gong J, Gong Y, Zou T, et al. A controllable perfusion microfluidic chip for facilitating the development of retinal ganglion cells in human retinal organoids. Lab Chip. 2023;23(17):3820–36. https://doi.org/10.1039/d3lc00054k. [published Online First: 2023/07/27].
33. Gong Y, He X, Li Q, et al. SCF/SCFR signaling plays an important role in the early morphogenesis and neurogenesis of human embryonic neural retina. Development. 2019;146(20). https://doi.org/10.1242/dev.174409. [published Online First: 2019/09/25].
34. Lyu J, Mu X. Genetic control of retinal ganglion cell genesis. Cell Mol Life Sci. 2021;78(9):4417–33. https://doi.org/10.1007/s00018-021-03814-w. [published Online First: 2021/03/31].
35. Wu F, Kaczynski TJ, Sethuramanujam S, et al. Two transcription factors, Pou4f2 and Isl1, are sufficient to specify the retinal ganglion cell fate. Proc Natl Acad Sci USA. 2015;112(13):E1559–68. https://doi.org/10.1073/pnas.1421535112. [published Online First: 2015/03/17].
36. Wu F, Bard JE, Kann J, et al. Single cell transcriptomics reveals lineage trajectory of retinal ganglion cells in wild-type and Atoh7-null retinas. Nat Commun. 2021;12(1):1465. https://doi.org/10.1038/s41467-021-21704-4. [published Online First: 2021/03/07].
37. Luo Z, Xu C, Li K, et al. Islet1 and Brn3 expression pattern study in human retina and hiPSC-Derived retinal organoid. Stem Cells Int. 2019;2019:8786396. https://doi.org/10.1155/2019/8786396. [published Online First: 2019/12/31].
38. Zhong Q, Cao M, Hu H, et al. One-Pot synthesis of highly stable CsPbBr(3)@SiO(2) Core-Shell nanoparticles. ACS Nano. 2018;12(8):8579–87. https://doi.org/10.1021/acsnano.8b04209. [published Online First: 2018/07/14].
39. Michalak M, Robert Parker JM, Opas M. Ca2 + signaling and calcium binding chaperones of the Endoplasmic reticulum. Cell Calcium. 2002;32(5–6):269–78. https://doi.org/10.1016/s0143416002001884. [published Online First: 2003/01/25].
40. Santulli G, Nakashima R, Yuan Q, et al. Intracellular calcium release channels: an update. J Physiol. 2017;595(10):3041–51. https://doi.org/10.1113/jp272781. [published Online First: 2017/03/18].
41. Chemaly ER, Troncone L, Lebeche D. SERCA control of cell death and survival. Cell Calcium. 2018;69:46–61. https://doi.org/10.1016/j.ceca.2017.07.001. [published Online First: 2017/07/28].
42. Zhou X, Fan GC, Ren X, et al. Overexpression of histidine-rich Ca-binding protein protects against ischemia/reperfusion-induced cardiac injury. Cardiovasc Res. 2007;75(3):487–97. https://doi.org/10.1016/j.cardiores.2007.04.005. [published Online First: 2007/05/15].
43. Preissler S, Rato C, Yan Y et al. Calcium depletion challenges Endoplasmic reticulum proteostasis by destabilising BiP-substrate complexes. Elife 2020;9 doi: 10.7554/eLife.62601 [published Online First: 2020/12/10].
44. Urra H, Dufey E, Lisbona F, et al. When ER stress reaches a dead end. Biochim Biophys Acta. 2013;1833(12):3507–17. https://doi.org/10.1016/j.bbamcr.2013.07.024. [published Online First: 2013/08/31].
45. Lu M, Lawrence DA, Marsters S, et al. Opposing unfolded-protein-response signals converge on death receptor 5 to control apoptosis. Science. 2014;345(6192):98–101. https://doi.org/10.1126/science.1254312. [published Online First: 2014/07/06].
46. Jimbo A, Fujita E, Kouroku Y, et al. ER stress induces caspase-8 activation, stimulating cytochrome C release and caspase-9 activation. Exp Cell Res. 2003;283(2):156–66. https://doi.org/10.1016/s0014-4827(02)00033-2. [published Online First: 2003/02/13].
47. Iurlaro R, Muñoz-Pinedo C. Cell death induced by Endoplasmic reticulum stress. Febs J. 2016;283(14):2640–52. https://doi.org/10.1111/febs.13598. [published Online First: 2015/11/21].
48. Laguesse S, Creppe C, Nedialkova DD, et al. A dynamic unfolded protein response contributes to the control of cortical neurogenesis. Dev Cell. 2015;35(5):553–67. [published Online First: 2015/12/15].
49. Kawada K, Iekumo T, Kaneko M, et al. [ER Stress-induced aberrant neuronal maturation and neurodevelopmental disorders]. Yakugaku Zasshi. 2016;136(6):811–5. https://doi.org/10.1248/yakushi.15-00292-3. [published Online First: 2016/06/03].
50. Mu X, Klein WH. A gene regulatory hierarchy for retinal ganglion cell specification and differentiation. Semin Cell Dev Biol. 2004;15(1):115–23. https://doi.org/10.1016/j.semcdb.2003.09.009. [published Online First: 2004/03/24].
51. Marquardt T, Ashery-Padan R, Andrejewski N, et al. Pax6 is required for the multipotent state of retinal progenitor cells. Cell. 2001;105(1):43–55. https://doi.org/10.1016/s0092-8674(01)00295-1. [published Online First: 2001/04/13].
52. Achberger K, Haderspeck JC, Kleger A, et al. Stem cell-based retina models. Adv Drug Deliv Rev. 2019;140:33–50. https://doi.org/10.1016/j.addr.2018.05.005. [published Online First: 2018/05/20].
53. Zhao H, Yan F. Retinal organoids: A Next-Generation platform for High-Throughput drug discovery. Stem Cell Rev Rep. 2023. https://doi.org/10.1007/s12015-023-10661-8. [published Online First: 2023/12/11].
54. Chakrabarty K, Nayak D, Debnath J, et al. Retinal organoids in disease modeling and drug discovery: opportunities and challenges. Surv Ophthalmol. 2023. https://doi.org/10.1016/j.survophthal.2023.09.003. [published Online First: 2023/10/02].
55. Xue Y, Lin B, Chen JT, et al. The prospects for retinal organoids in treatment of retinal diseases. Asia Pac J Ophthalmol (Phila). 2022;11(4):314–27. https://doi.org/10.1097/apo.0000000000000538. [published Online First: 2022/08/31].
56. Mei L, Xie R, Zhu S, et al. Neurotoxicity study of lead-based perovskite nanoparticles. Nano Today. 2023;50:101830. https://doi.org/10.1016/j.nantod.2023.101830.
57. He R, Ding X, Zhang T, et al. Study on myocardial toxicity induced by lead halide perovskites nanoparticles. Nanotoxicology. 2023;17(5):449–70. https://doi.org/10.1080/17435390.2023.2255269. [published Online First: 2023/09/09].
58. Mason LH, Harp JP, Han DY. Pb neurotoxicity: neuropsychological effects of lead toxicity. Biomed Res Int. 2014;2014:840547. https://doi.org/10.1155/2014/840547. [published Online First: 2014/02/12].
59. Tasin FR, Ahmed A, Halder D, et al. On-going consequences of in utero exposure of Pb: an epigenetic perspective. J Appl Toxicol. 2022;42(10):1553–69. https://doi.org/10.1002/jat.4287. [published Online First: 2022/01/14].
60. Chaney SY, Mukherjee S, Giddabasappa A, et al. Increased proliferation of late-born retinal progenitor cells by gestational lead exposure delays rod and bipolar cell differentiation. Mol Vis. 2016;22:1468–89. [published Online First: 2017/01/05].
61. Fox DA, Katz LM, Farber DB. Low level developmental lead exposure decreases the sensitivity, amplitude and Temporal resolution of rods. Neurotoxicology. 1991;12(4):641–54. [published Online First: 1991/01/01].
62. Kay JN. Radial migration: retinal neurons hold on for the ride. J Cell Biol. 2016;215(2):147–49. https://doi.org/10.1083/jcb.201609135. [published Online First: 2016/11/05].
63. Hoon M, Okawa H, Della Santina L, et al. Functional architecture of the retina: development and disease. Prog Retin Eye Res. 2014;42:44–84. https://doi.org/10.1016/j.preteyeres.2014.06.003. [published Online First: 2014/07/02].
64. Amini R, Rocha-Martins M, Norden C. Neuronal migration and lamination in the vertebrate retina. Front Neurosci. 2017;11:742. https://doi.org/10.3389/fnins.2017.00742. [published Online First: 2018/01/30].
65. Tang F, Li L, Chen D. Mesoporous silica nanoparticles: synthesis, biocompatibility and drug delivery. Adv Mater. 2012;24(12):1504–34. https://doi.org/10.1002/adma.201104763. [published Online First: 2012/03/02].
66. Xu B, Li S, Shi R, et al. Multifunctional mesoporous silica nanoparticles for biomedical applications. Signal Transduct Target Ther. 2023;8(1):435. https://doi.org/10.1038/s41392-023-01654-7. [published Online First: 2023/11/24].
67. Chia SL, Leong DT. Reducing ZnO nanoparticles toxicity through silica coating. Heliyon. 2016;2(10):e00177. https://doi.org/10.1016/j.heliyon.2016.e00177. [published Online First: 2016/11/05].
68. Camaioni A, Massimiani M, Lacconi V, et al. Silica encapsulation of ZnO nanoparticles reduces their toxicity for cumulus cell-oocyte-complex expansion. Part Fibre Toxicol. 2021;18(1):33. https://doi.org/10.1186/s12989-021-00424-z. [published Online First: 2021/09/05].
69. Toth AB, Shum AK, Prakriya M. Regulation of neurogenesis by calcium signaling. Cell Calcium. 2016;59(2–3):124–34. https://doi.org/10.1016/j.ceca.2016.02.011. [published Online First: 2016/03/30].
70. Mekahli D, Bultynck G, Parys JB, et al. Endoplasmic-reticulum calcium depletion and disease. Cold Spring Harb Perspect Biol. 2011;3(6). https://doi.org/10.1101/cshperspect.a004317. [published Online First: 2011/03/29].
71. Komoike Y, Matsuoka M. Developmental adverse effects of trace amounts of lead: evaluation using zebrafish model. Front Pharmacol. 2022;13:1014912. https://doi.org/10.3389/fphar.2022.1014912. [published Online First: 2022/10/11].

72. Kroeger H, Chiang WC, Felden J, et al. ER stress and unfolded protein response in ocular health and disease. Febs J. 2019;286(2):399–412. https://doi.org/10.1111/febs.14522. [published Online First: 2018/05/29].
73. Jing G, Wang JJ, Zhang SX. ER stress and apoptosis: a new mechanism for retinal cell death. Exp Diabetes Res. 2012;2012:589589. https://doi.org/10.1155/2012/589589. [published Online First: 2012/01/05].
74. Zhang SX, Wang JJ, Starr CR, et al. The Endoplasmic reticulum: homeostasis and crosstalk in retinal health and disease. Prog Retin Eye Res. 2024;98:101231. https://doi.org/10.1016/j.preteyeres.2023.101231. [published Online First: 2023/12/14].

Publisher's note